Sulphur-rich Functionalized Calix[4]arenes for selective complexation of Hg^{2+} over Cu^{2+}, Zn^{2+} and Cd^{2+}

Bachir Bensenane,[a,b] Zouhair Asfari,[a] Carlos Platas-Iglesias,[c*] David Esteban-Gómez,[c] Fatiha Djafri,[b] Mourad Elhabiri[d*] and Loïc J. Charbonnière[a*]

a. Laboratoire d'Ingénierie Moléculaire Appliquée à l'Analyse (LIMAA), IPHC - UMR 7178 – CNRS, ECPM, Bât R1N0, 25 rue Becquerel, 67087 Strasbourg Cedex 02, France. Email: l.Charbonn@unistra.fr

b. Laboratoire de chimie des matériaux, Faculté des sciences, Université d'Oran, B.P. 1524 El-Menouer, 31000 Oran, Algeria.

c. Universidade da Coruña,Centro de Investigacións Científicas Avanzadas (CICA) and Departamento de Química Fundamental, Facultade de Ciencias,, 15071, A Coruña, Galicia, Spain. Email: carlos.platas.iglesias@udc.es

d. Laboratoire de Chimie Bioorganique et Médicinale, UMR 7509 – CNRS, ECPM, 25, rue Becquerel, 67087 Strasbourg Cedex 02, France. E-mail: elhabiri@unistra.fr

Supplementary information (30 pages including this one)

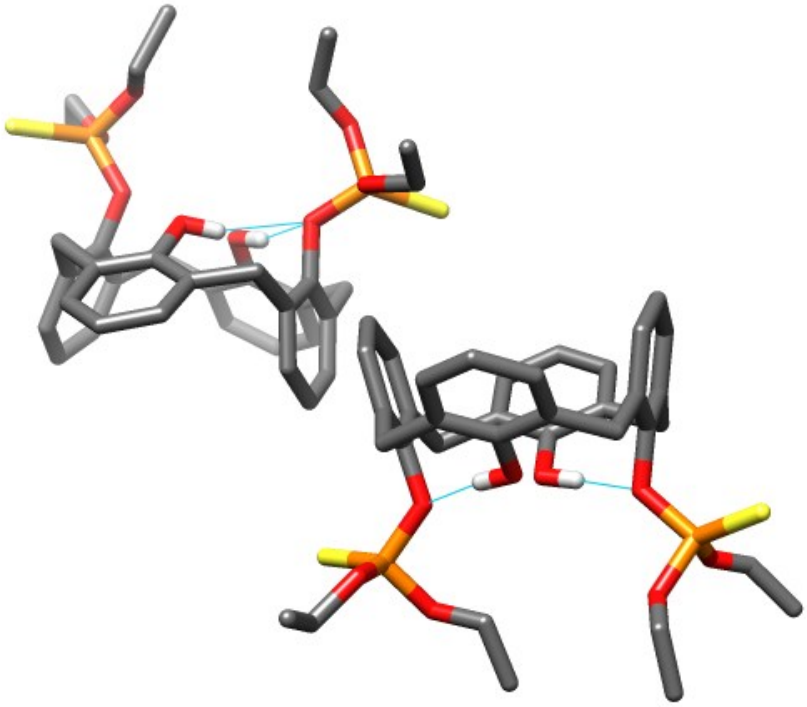

Figure S1. Representation of the unit cell of the X-Ray crystal structure of **L1**.

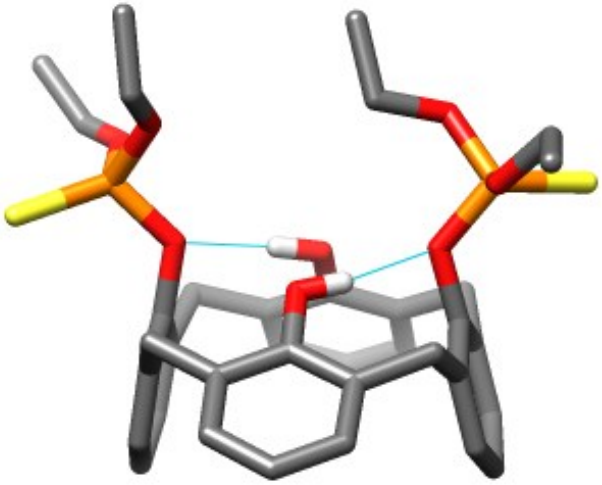

Figure S2. X-Ray crystal structure of **L1**.

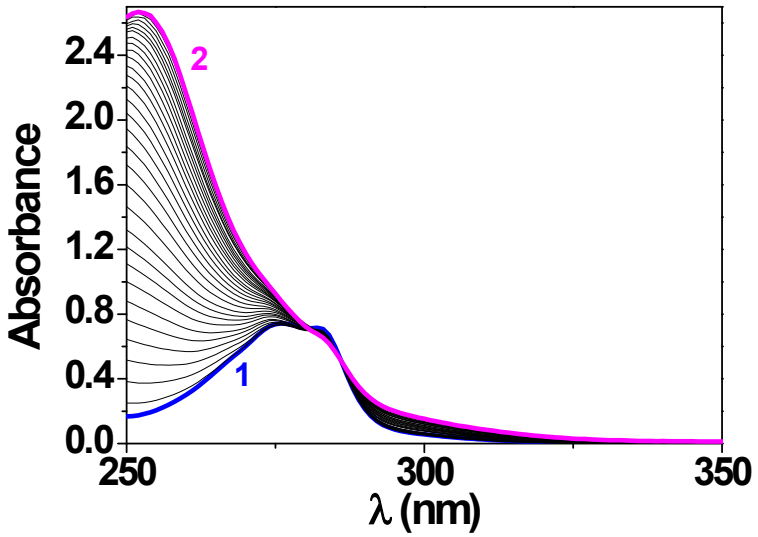

(A)

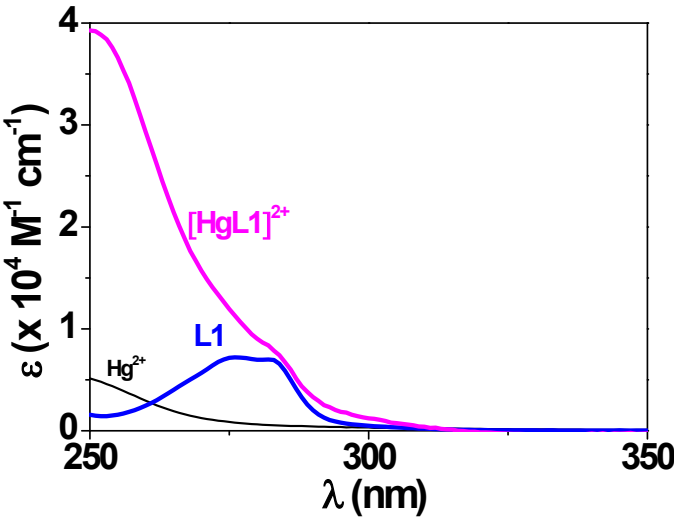

(B)

Figure S3. (a) Absorption spectrophotometric titration of **L1** by Hg^{2+}. Solvent: CH_3CN/CH_2Cl_2 (1/1 *v/v*); I = 0.01 M $(C_2H_5)_4NNO_3$); T = 25.0(2)°C; □ = 1 cm; $[\mathbf{L1}]_0 = 10^{-4}$ M; (1) $[Hg^{2+}]_0/[\mathbf{L1}]_0 = 0$; (2) $[Hg^{2+}]_0/[\mathbf{L1}]_0 = 5$. The spectra are not corrected from the dilution effects. (b) Absorption electronic spectra of **L1** and its Hg^{2+} monochelate.

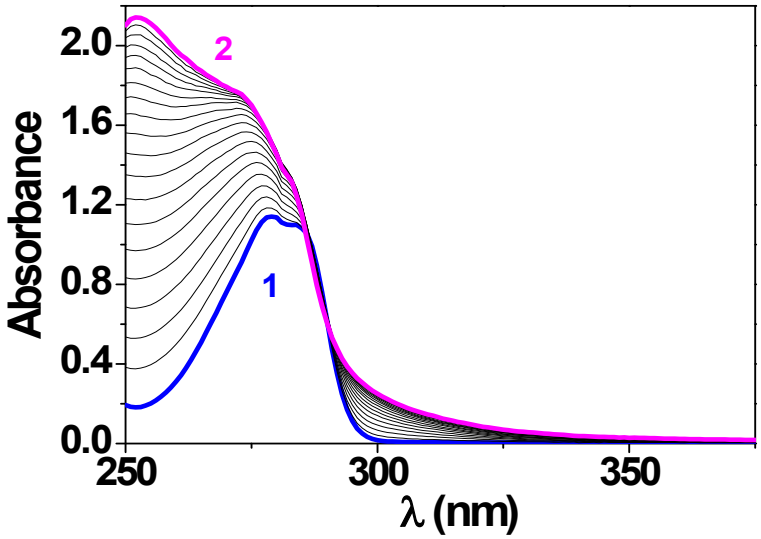

(A)

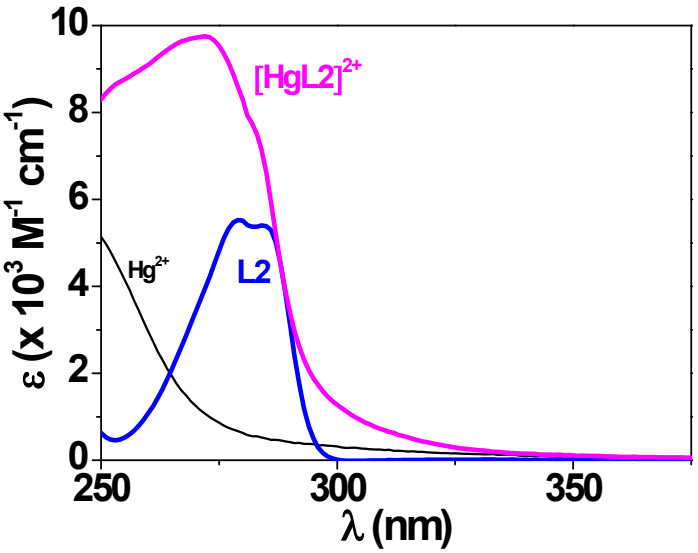

(B)

Figure S4. (a) Absorption spectrophotometric titration of **L2** by Hg^{2+}. Solvent: CH_3CN/CH_2Cl_2 (1/1 *v/v*); I = 0.01 M $(C_2H_5)_4NNO_3$); T = 25.0(2)°C; □ = 1 cm; $[\mathbf{L2}]_0 = 10^{-4}$ M; (1) $[Hg^{2+}]_0/[\mathbf{L2}]_0 = 0$; (2) $[Hg^{2+}]_0/[\mathbf{L2}]_0 = 2$. The spectra are not corrected from the dilution effects. (b) Absorption electronic spectra of **L2** and its Hg^{2+} monochelate.

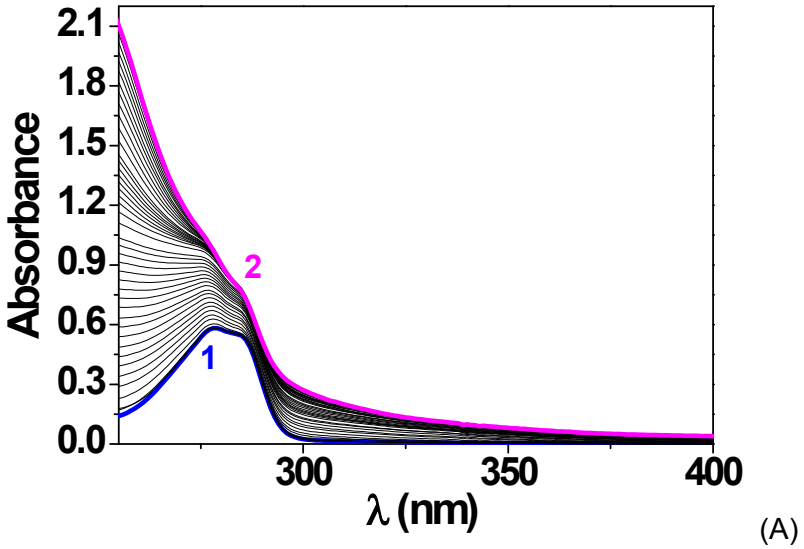

(A)

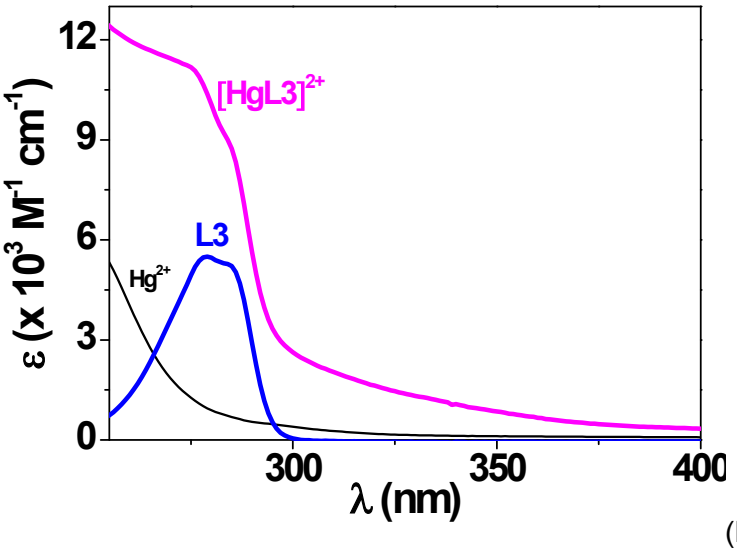

(B)

Figure S5. (a) Absorption spectrophotometric titration of **L3** by Hg^{2+}. Solvent: CH_3CN/CH_2Cl_2 (1/1 *v/v*); I = 0.01 M $(C_2H_5)_4NNO_3$); T = 25.0(2)°C; □ = 1 cm; $[\mathbf{L3}]_0 = 10^{-4}$ M; (1) $[Hg^{2+}]_0/[\mathbf{L3}]_0 = 0$; (2) $[Hg^{2+}]_0/[\mathbf{L3}]_0 = 3$. The spectra are not corrected from the dilution effects. (b) Absorption electronic spectra of **L3** and its Hg^{2+} monochelate.

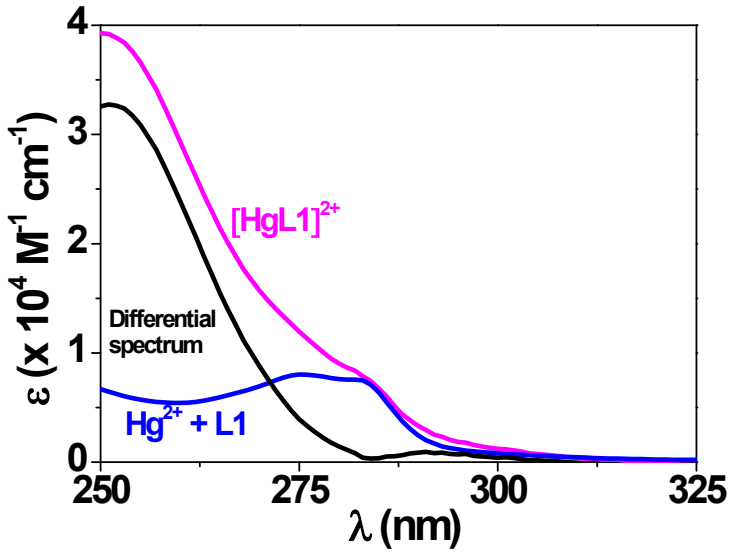

(A)

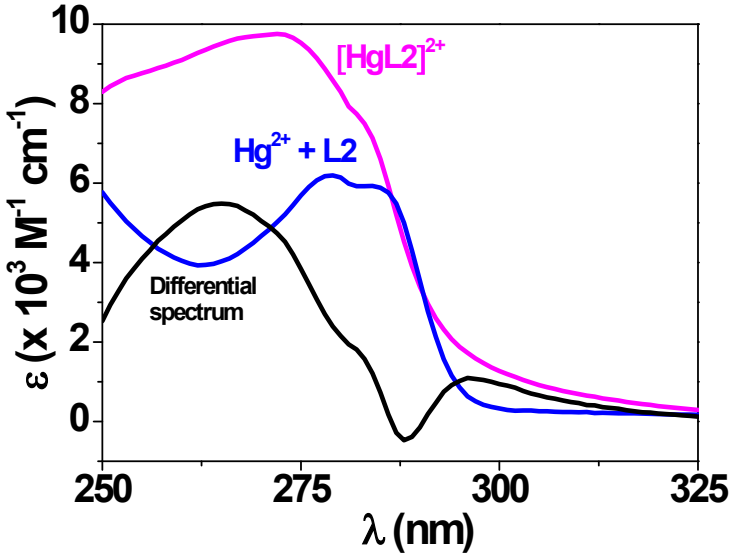

(B)

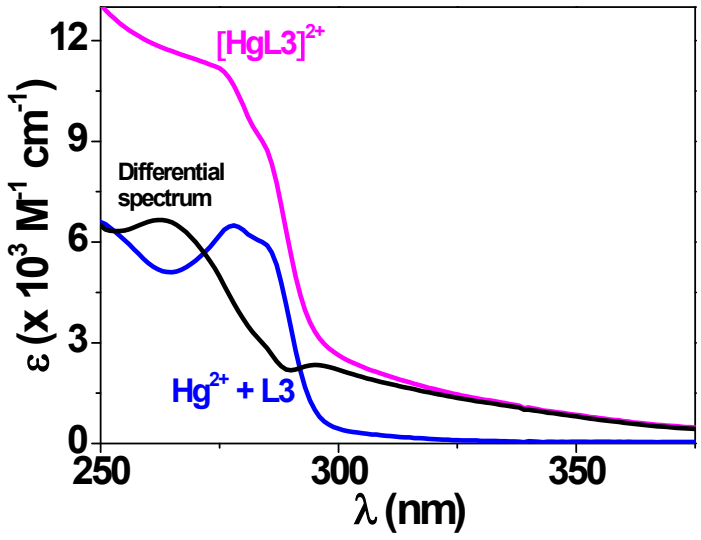

(C)

Figure S6. Differential Electronic spectra of the mercuric complexes with ligands (a) **L1**, (b) **L2**, and (c) **L3**. Solvent: CH_3CN/CH_2Cl_2 (1/1 *v/v*); $I = 0.01$ M $(C_2H_5)_4NNO_3$); $T = 25.0(2)$ °C.

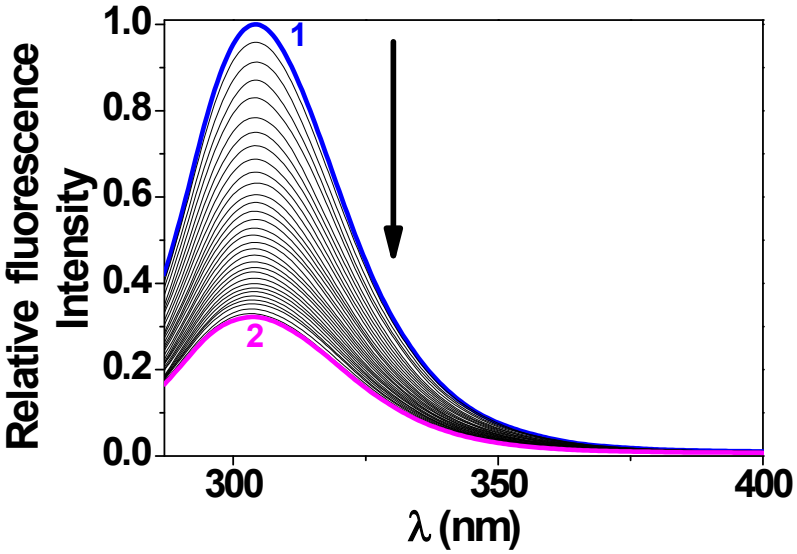

Figure S7. Spectrofluorimetric titration of ligand **L1** (λ_{exc} = 289 nm) by Hg^{2+}. Solvent: CH_3CN/CH_2Cl_2 (1/1 *v/v*); I = 0.01 M $(C_2H_5)_4NNO_3$); T = 25.0(2) °C; □ = 1 cm; $[\mathbf{L1}]_0 = 10^{-4}$ M; (1) $[Hg^{2+}]_0/[\mathbf{L1}]_0 = 0$; (2) $[Hg^{2+}]_0/[\mathbf{L1}]_0 = 2$. Emission spectra not corrected from dilution effects.

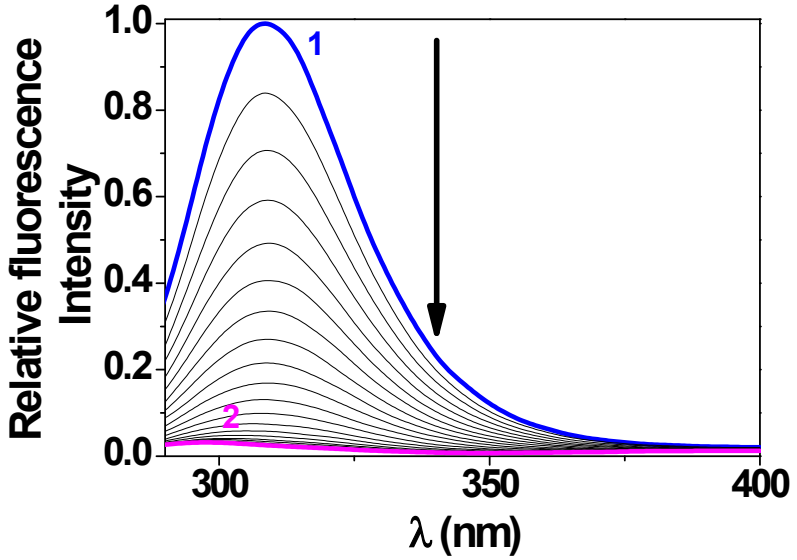

Figure S8. Spectrofluorimetric titration of ligand **L2** (λ_{exc} = 289 nm) by Hg^{2+}. Solvent: CH_3CN/CH_2Cl_2 (1/1 *v/v*); I = 0.01 M $(C_2H_5)_4NNO_3$); T = 25.0(2) °C; □ = 1 cm; $[\mathbf{L2}]_0 = 10^{-4}$ M; (1) $[Hg^{2+}]_0/[\mathbf{L2}]_0 = 0$; (2) $[Hg^{2+}]_0/[\mathbf{L2}]_0 = 2$. Emission spectra not corrected from dilution effects.

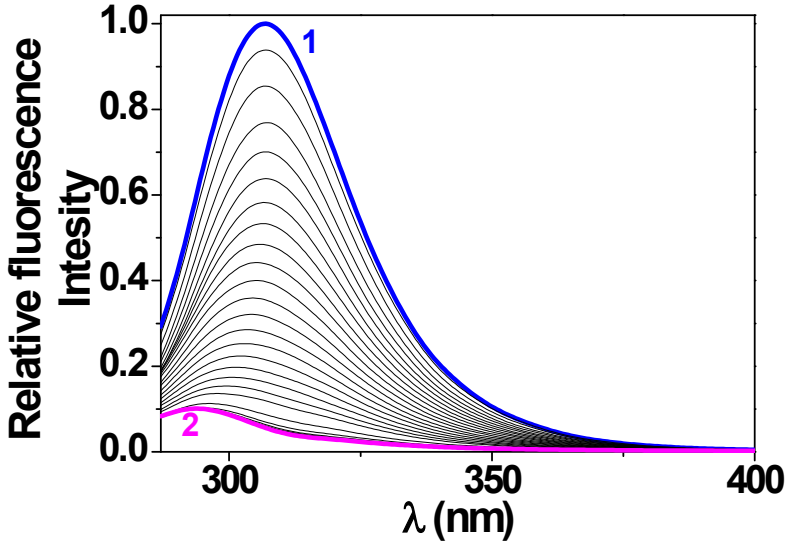

Figure S9. Spectrofluorimetric titration of ligand **L3** (λ_{exc} = 287 nm) by Hg^{2+}. Solvent: CH_3CN/CH_2Cl_2 (1/1 *v/v*); *I* = 0.01 M $(C_2H_5)_4NNO_3$); *T* = 25.0(2) °C; □ = 1 cm; $[\mathbf{L3}]_0 = 10^{-4}$ M; (1) $[Hg^{2+}]_0/[\mathbf{L3}]_0 = 0$; (2) $[Hg^{2+}]_0/[\mathbf{L3}]_0 = 3$. Emission spectra not corrected from dilution effects.

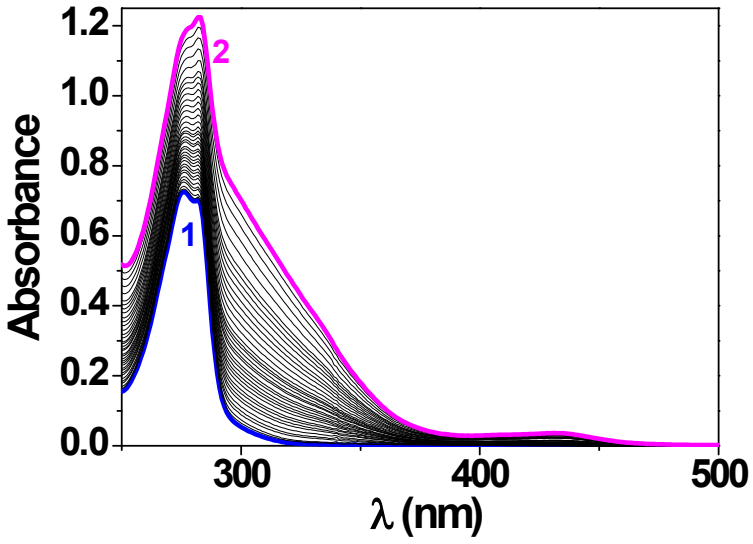

(A)

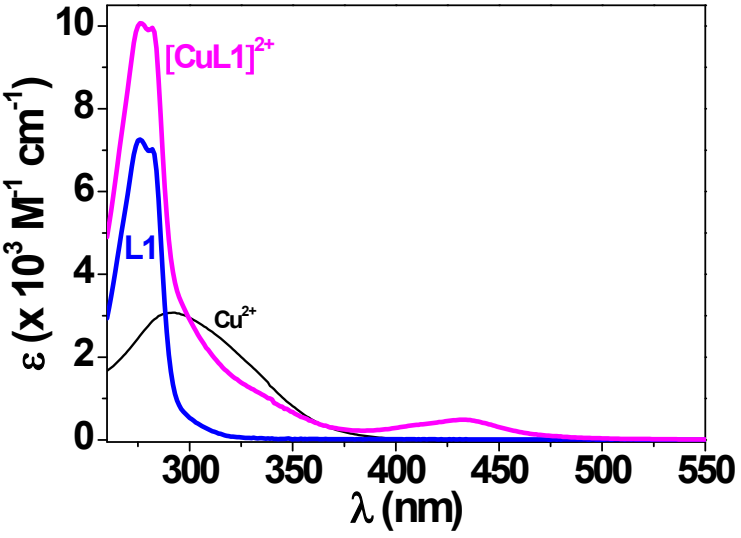

(B)

Figure S10. (a) Absorption spectrophotometric titration of **L1** by Cu^{2+}. Solvent: CH_3CN/CH_2Cl_2 (1/1 *v/v*); I = 0.01 M $(C_2H_5)_4NNO_3$); T = 25.0(2)°C; □ = 1 cm; $[\mathbf{L1}]_0 = 10^{-4}$ M; (1) $[Cu^{2+}]_0/[\mathbf{L1}]_0 = 0$; (2) $[Cu^{2+}]_0/[\mathbf{L1}]_0 = 2.5$. The spectra are not corrected from the dilution effects. (b) Absorption electronic spectra of **L1** and its cupric monochelate.

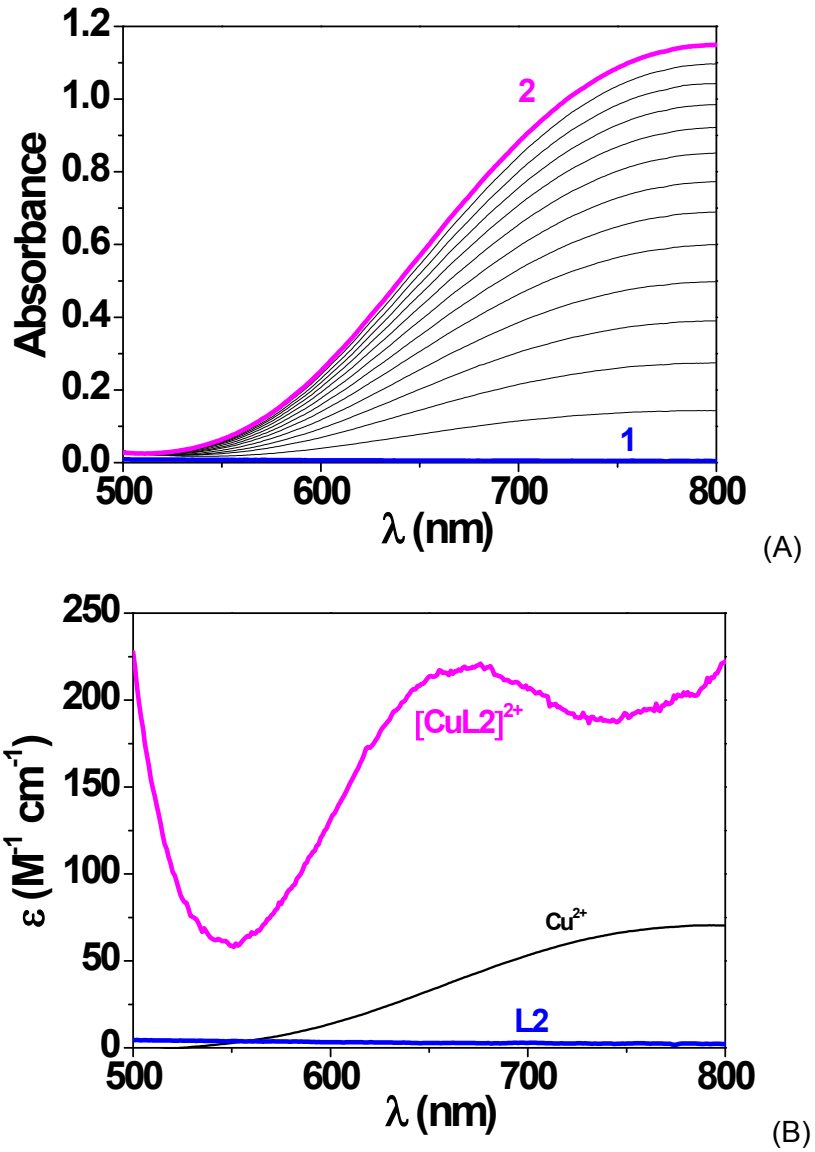

Figure S11. (a) Absorption spectrophotometric titration of **L2** by Cu^{2+}. Solvent: CH_3CN/CH_2Cl_2 (1/1 *v/v*); I = 0.01 M $(C_2H_5)_4NNO_3$); T = 25.0(2)°C; □ = 1 cm; $[\mathbf{L2}]_0 = 10^{-3}$ M; (1) $[Cu^{2+}]_0/[\mathbf{L2}]_0 = 0$; (2) $[Cu^{2+}]_0/[\mathbf{L2}]_0 = 13$. The spectra are not corrected from the dilution effects. (b) Absorption electronic spectra of **L2** and its cupric monochelate.

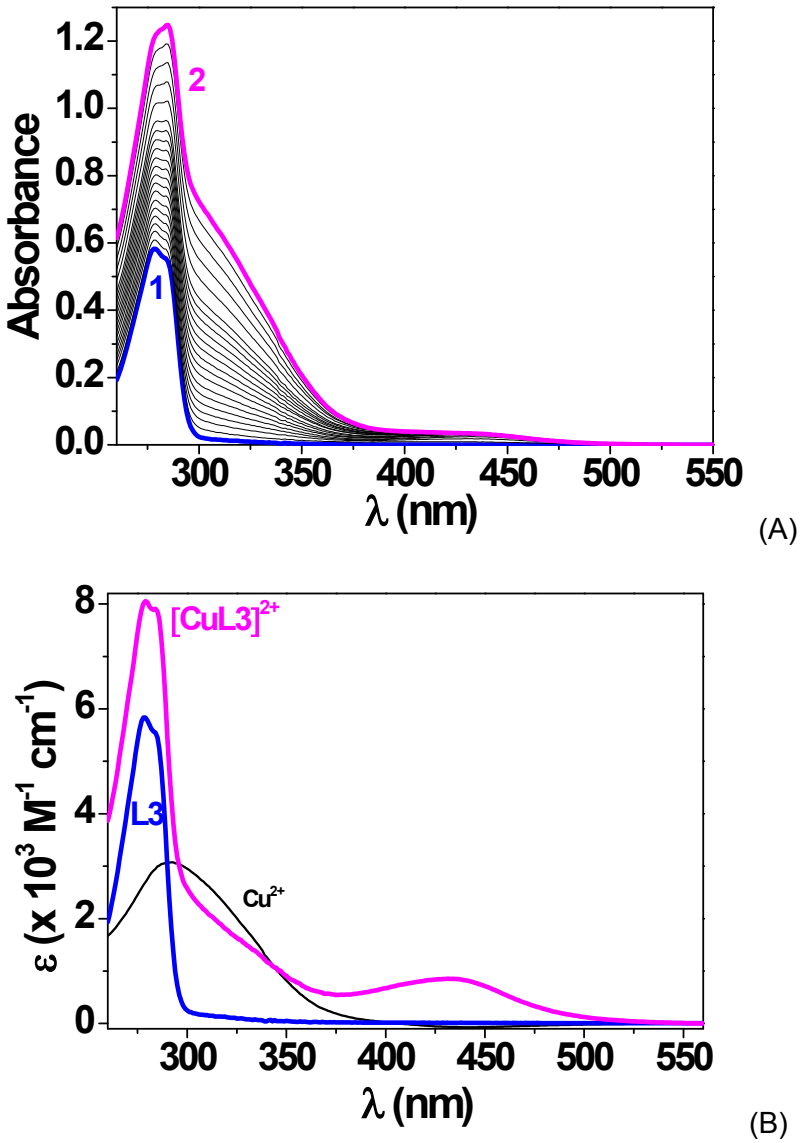

Figure S12. (a) Absorption spectrophotometric titration of **L3** by Cu^{2+}. Solvent: CH_3CN/CH_2Cl_2 (1/1 *v/v*); I = 0.01 M $(C_2H_5)_4NNO_3$); T = 25.0(2)°C; □ = 1 cm; $[\mathbf{L3}]_0 = 10^{-4}$ M; (1) $[Cu^{2+}]_0/[\mathbf{L3}]_0 = 0$; (2) $[Cu^{2+}]_0/[\mathbf{L3}]_0 = 2.5$. The spectra are not corrected from the dilution effects. (b) Absorption electronic spectra of **L3** and its cupric monochelate.

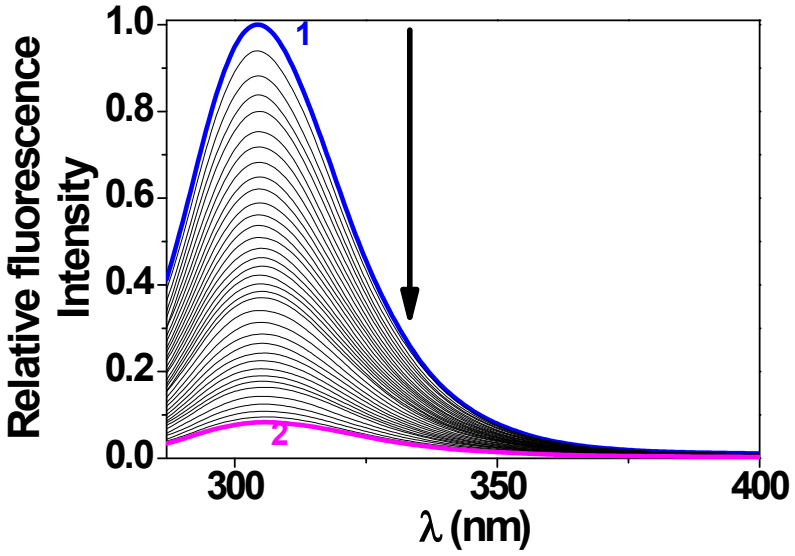

Figure S13. Spectrofluorimetric titration of ligand **L1** (λ_{exc} = 287 nm) by Cu^{2+}. Solvent: CH_3CN/CH_2Cl_2 (1/1 *v/v*); I = 0.01 M $(C_2H_5)_4NNO_3$); T = 25.0(2) °C; □ = 1 cm; $[\mathbf{L1}]_0 = 10^{-4}$ M; (1) $[Cu^{2+}]_0/[\mathbf{L1}]_0 = 0$; (2) $[Cu^{2+}]_0/[\mathbf{L1}]_0 = 2.5$. Emission spectra not corrected from dilution effects.

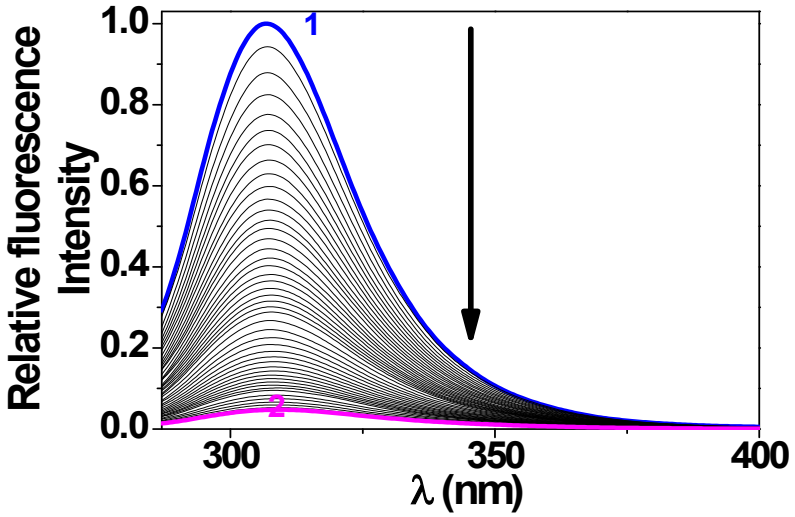

Figure S14. Spectrofluorimetric titration of ligand **L3** (λ_{exc} = 287 nm) by Cu^{2+}. Solvent: CH_3CN/CH_2Cl_2 (1/1 *v/v*); I = 0.01 M $(C_2H_5)_4NNO_3$); T = 25.0(2) °C; □ = 1 cm; $[\mathbf{L3}]_0 = 10^{-4}$ M; (1) $[Cu^{2+}]_0/[\mathbf{L3}]_0 = 0$; (2) $[Cu^{2+}]_0/[\mathbf{L3}]_0 = 3.7$. Emission spectra not corrected from dilution effects.

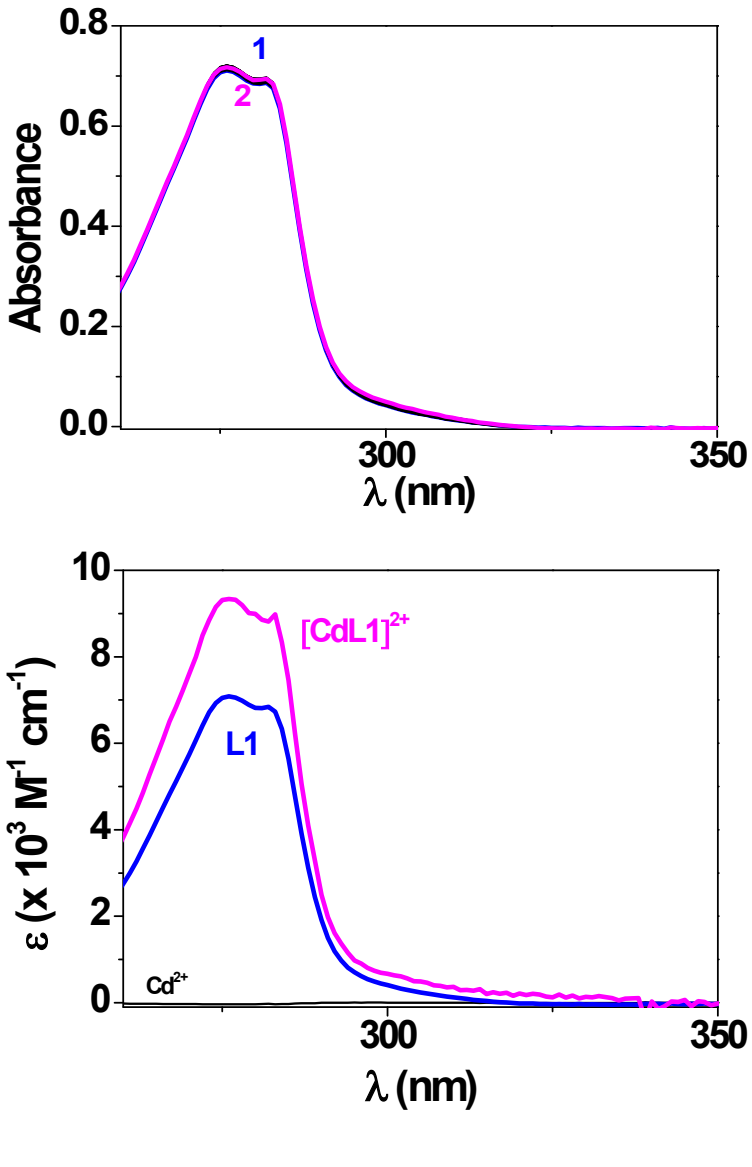

Figure S15. (a) Absorption spectrophotometric titration of **L1** by Cd^{2+}. Solvent: CH_3CN/CH_2Cl_2 (1/1 *v/v*); I = 0.01 M $(C_2H_5)_4NNO_3$); T = 25.0(2)°C; □ = 1 cm; $[\mathbf{L1}]_0 = 10^{-4}$ M; (1) $[Cd^{2+}]_0/[\mathbf{L1}]_0 = 0$; (2) $[Cd^{2+}]_0/[\mathbf{L1}]_0 = 9.5$. The spectra are not corrected from the dilution effects. (b) Absorption electronic spectra of **L1** and its Cd^{2+} monochelate.

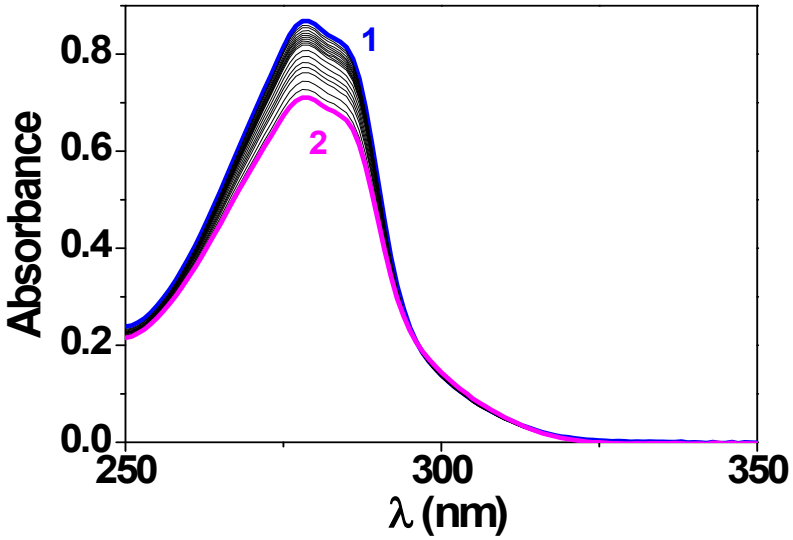

(A)

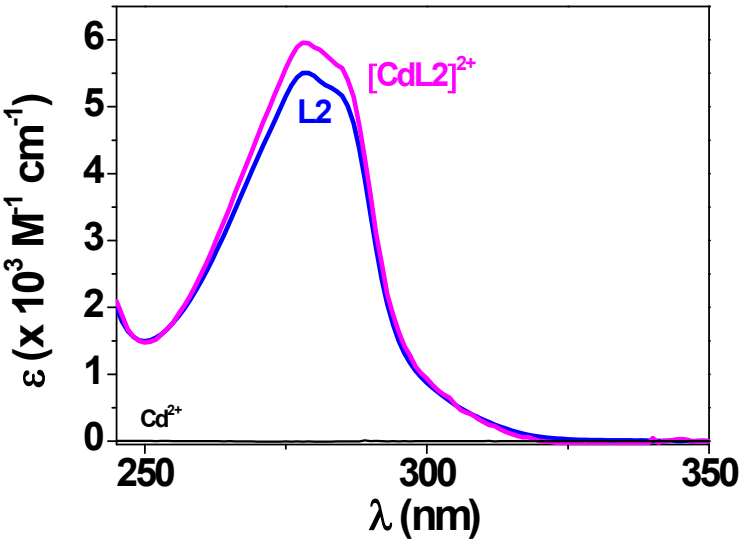

(B)

Figure S16. (a) Absorption spectrophotometric titration of **L2** by Cd^{2+}. Solvent: CH_3CN/CH_2Cl_2 (1/1 *v/v*); I = 0.01 M $(C_2H_5)_4NNO_3$); T = 25.0(2)°C; □ = 1 cm; $[\mathbf{L2}]_0 = 1.58 \times 10^{-4}$ M; (1) $[Cd^{2+}]_0/[\mathbf{L2}]_0 = 0$; (2) $[Cd^{2+}]_0/[\mathbf{L2}]_0 = 2.53$. The spectra are not corrected from the dilution effects. (b) Absorption electronic spectra of **L2** and its Cd^{2+} monochelate.

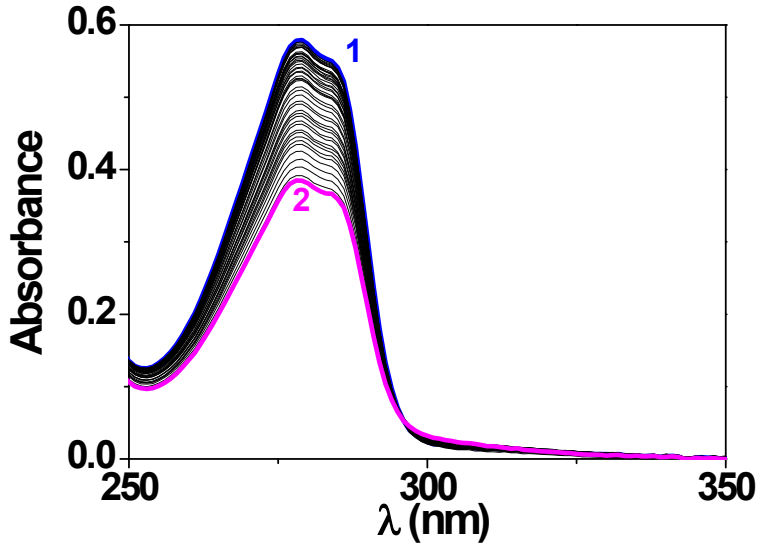

(A)

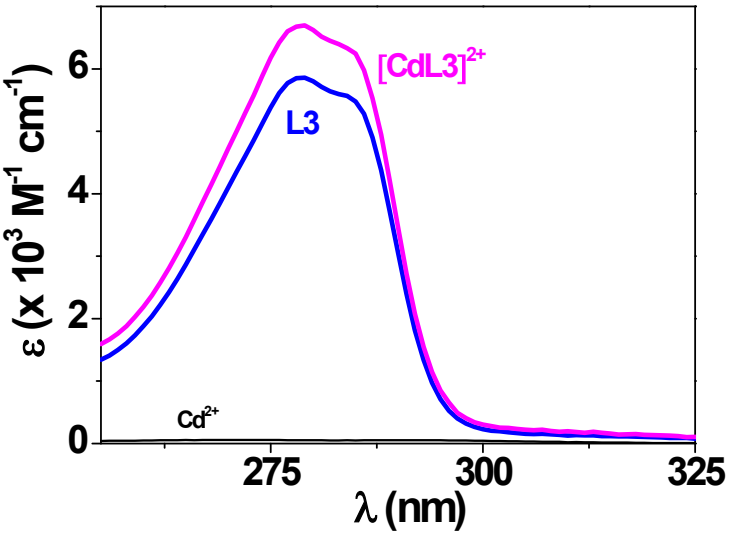

(B)

Figure S17. (a) Absorption spectrophotometric titration of **L3** by Cd^{2+}. Solvent: CH_3CN/CH_2Cl_2 (1/1 *v/v*); *I* = 0.01 M $(C_2H_5)_4NNO_3$); *T* = 25.0(2)°C; □ = 1 cm; $[\mathbf{L3}]_0 = 10^{-4}$ M; (1) $[Cd^{2+}]_0/[\mathbf{L3}]_0 = 0$; (2) $[Cd^{2+}]_0/[\mathbf{L3}]_0 = 5$. The spectra are not corrected from the dilution effects. (b) Absorption electronic spectra of **L3** and its Cd^{2+} monochelate.

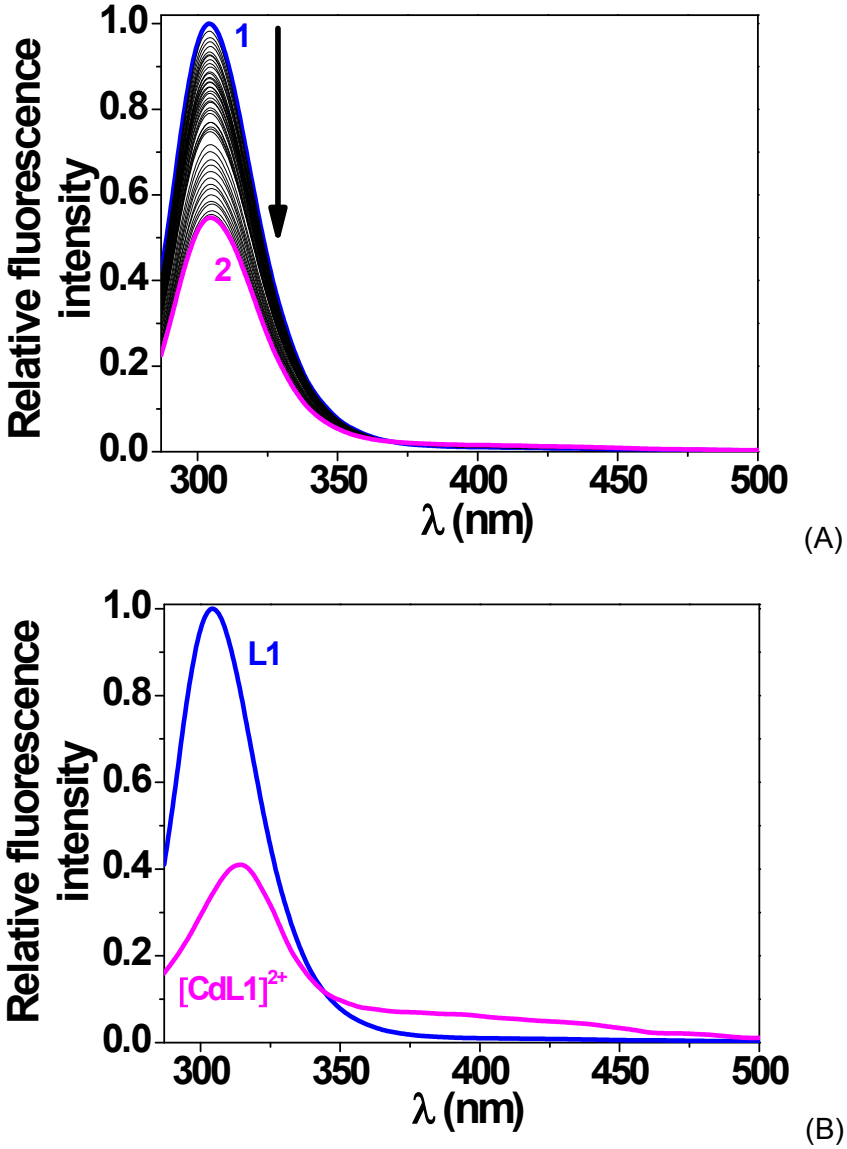

Figure S18. (A) Spectrofluorimetric titration of ligand **L1** (λ_{exc} = 289 nm) by Cd^{2+}. Solvent: CH_3CN/CH_2Cl_2 (1/1 *v/v*); I = 0.01 M $(C_2H_5)_4NNO_3$); T = 25.0(2) °C; □ = 1 cm; $[\mathbf{L1}]_0 = 10^{-4}$ M; (1) $[Cd^{2+}]_0/[\mathbf{L1}]_0 = 0$; (2) $[Cd^{2+}]_0/[\mathbf{L1}]_0 = 2.5$. Emission spectra not corrected from dilution effects. (B) Reconstituted fluorescence emission spectra of **L1** and its Cd^{2+} monochelate.

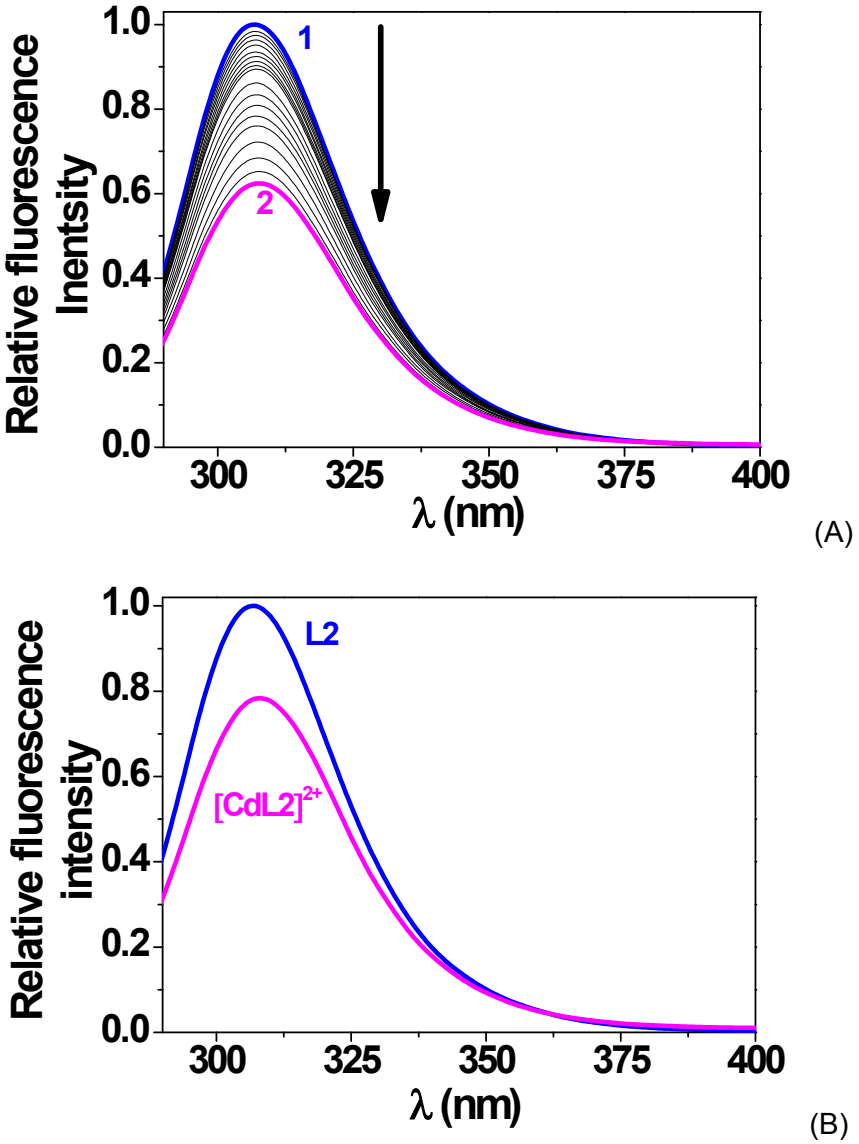

Figure S19. (A) Spectrofluorimetric titration of ligand **L2** (λ_{exc} = 287 nm) by Cd^{2+}. Solvent: CH_3CN/CH_2Cl_2 (1/1 *v/v*); I = 0.01 M $(C_2H_5)_4NNO_3$); T = 25.0(2) °C; □ = 1 cm; $[\mathbf{L2}]_0 = 1.58 \times 10^{-4}$ M; (1) $[Cd^{2+}]_0/[\mathbf{L2}]_0 = 0$; (2) $[Cd^{2+}]_0/[\mathbf{L2}]_0 = 5$. Emission spectra not corrected from dilution effects. (B) Reconstituted fluorescence emission spectra of **L2** and its Cd^{2+} monochelate.

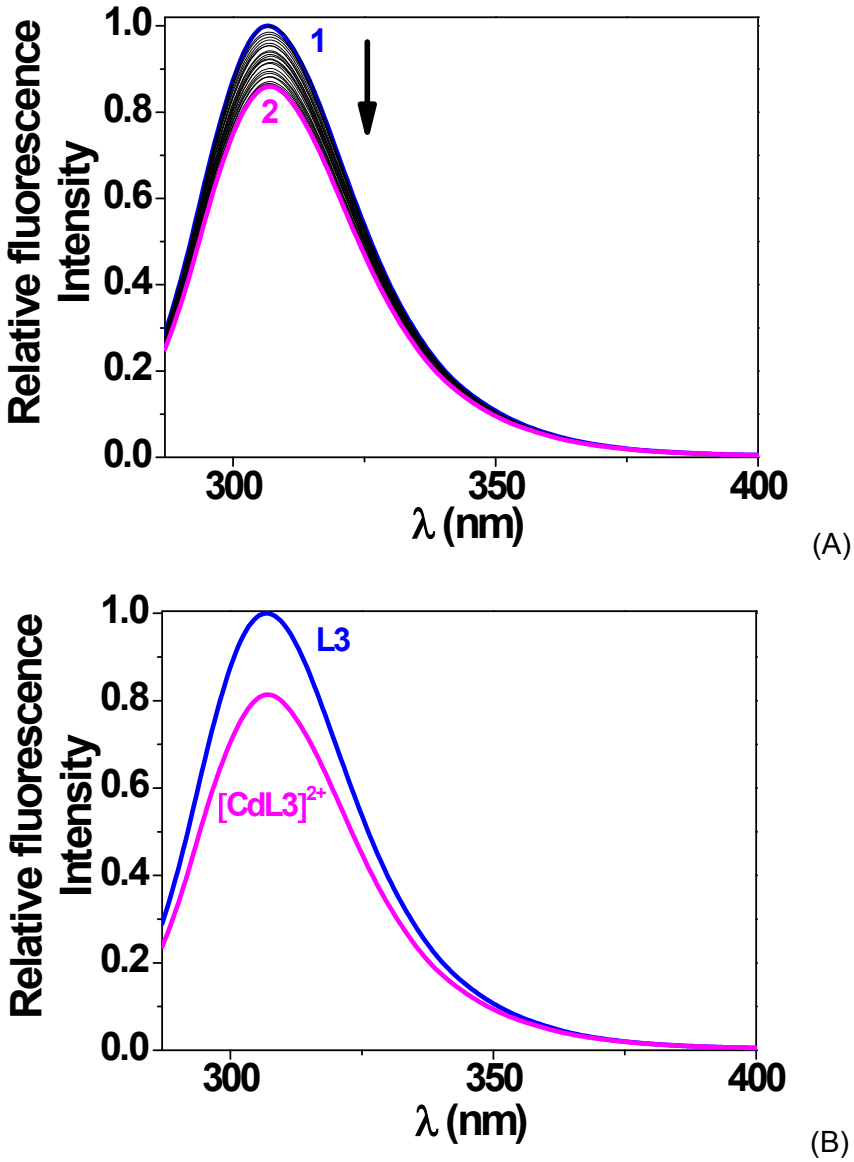

Figure S20. (A) Spectrofluorimetric titration of ligand **L3** (λ_{exc} = 287 nm) by Cd^{2+}. Solvent: CH_3CN/CH_2Cl_2 (1/1 *v/v*); I = 0.01 M $(C_2H_5)_4NNO_3$); T = 25.0(2) °C; □ = 1 cm; $[\mathbf{L3}]_0 = 10^{-4}$ M; (1) $[Cd^{2+}]_0/[\mathbf{L3}]_0$ = 0; (2) $[Cd^{2+}]_0/[\mathbf{L3}]_0$ = 7. Emission spectra not corrected from dilution effects. (B) Reconstituted fluorescence emission spectra of **L3** and its Cd^{2+} monochelate.

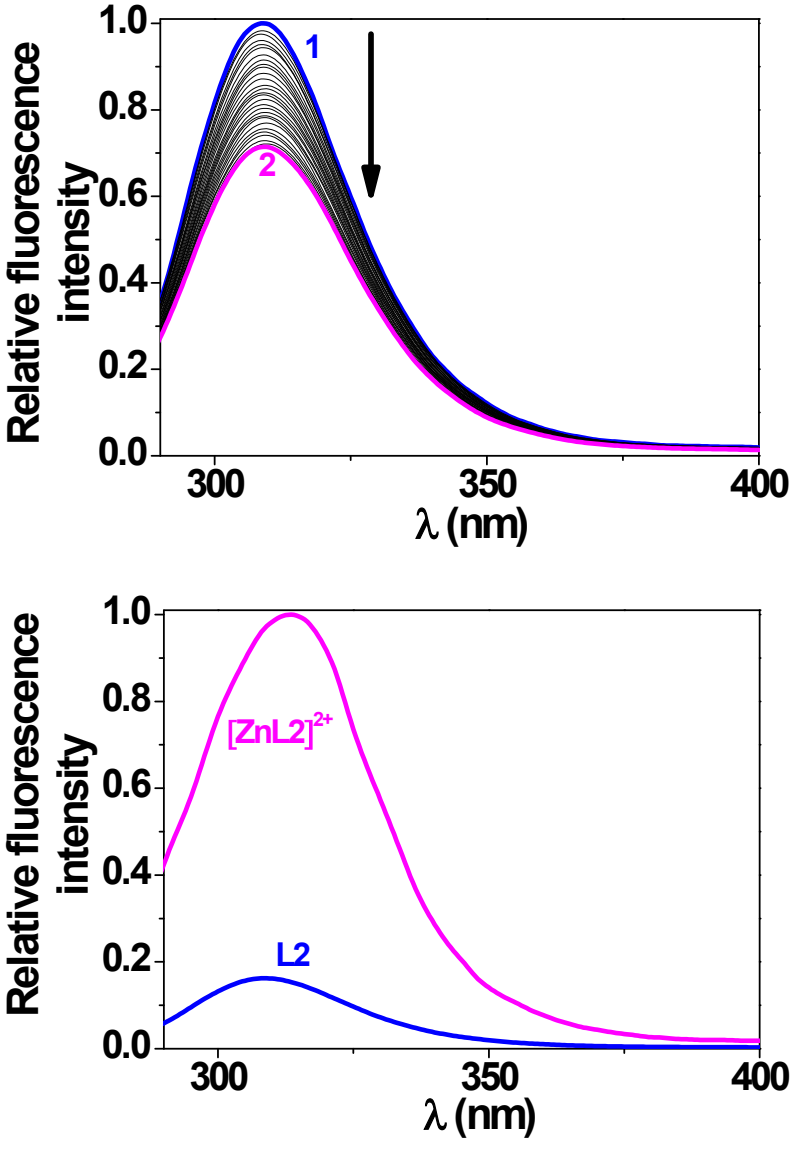

Figure S21. (A) Spectrofluorimetric titration of ligand **L2** (λ_{exc} = 289 nm) by Zn^{2+}. Solvent: CH_3CN/CH_2Cl_2 (1/1 *v/v*); I = 0.01 M $(C_2H_5)_4NNO_3$); T = 25.0(2) °C; □ = 1 cm; $[\mathbf{L2}]_0 = 1.58 \times 10^{-4}$ M; (1) $[Zn^{2+}]_0/[\mathbf{L2}]_0 = 0$; (2) $[Zn^{2+}]_0/[\mathbf{L2}]_0 = 85.4$. Emission spectra not corrected from dilution effects. (B) Reconstituted fluorescence emission spectra of **L2** and its Zn^{2+} monochelate.

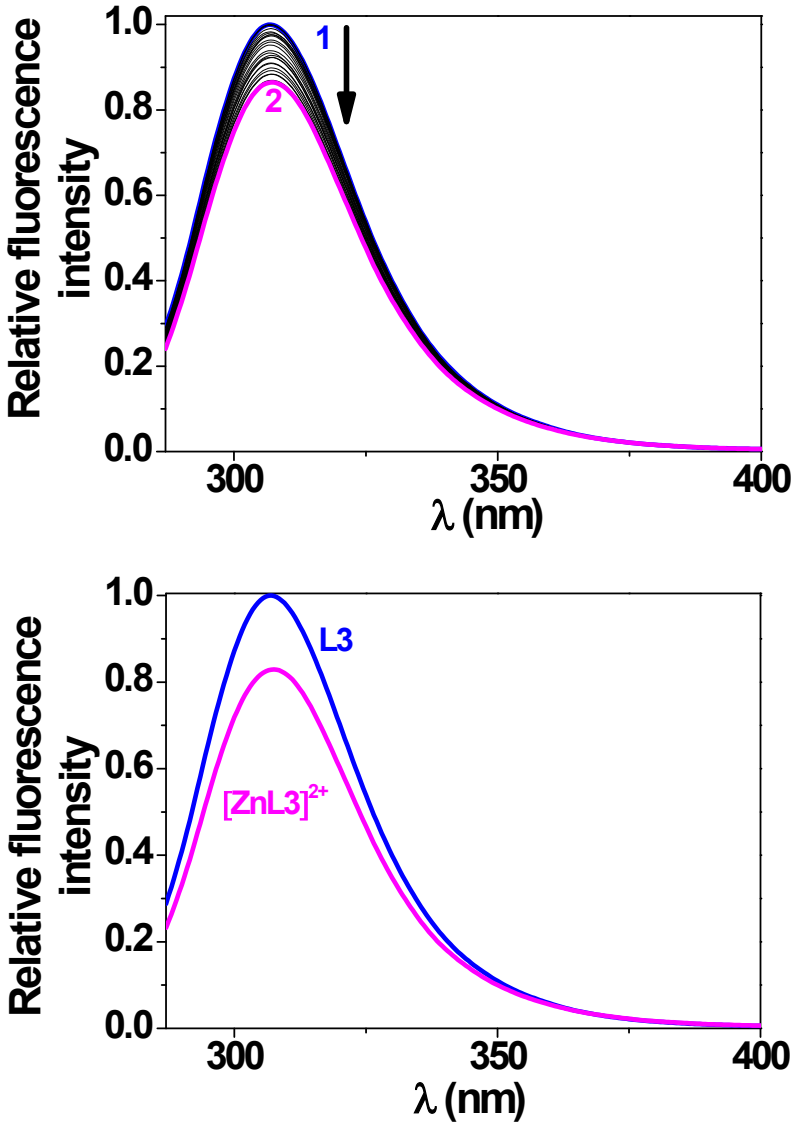

Figure S22. (A) Spectrofluorimetric titration of ligand **L3** (λ_{exc} = 287 nm) by Zn^{2+}. Solvent: CH_3CN/CH_2Cl_2 (1/1 *v/v*); I = 0.01 M $(C_2H_5)_4NNO_3$); T = 25.0(2) °C; □ = 1 cm; $[\mathbf{L3}]_0 = 10^{-4}$ M; (1) $[Zn^{2+}]_0/[\mathbf{L3}]_0 = 0$; (2) $[Zn^{2+}]_0/[\mathbf{L3}]_0 = 9.4$. Emission spectra not corrected from dilution effects. (B) Reconstituted fluorescence emission spectra of **L3** and its Zn^{2+} monochelate.

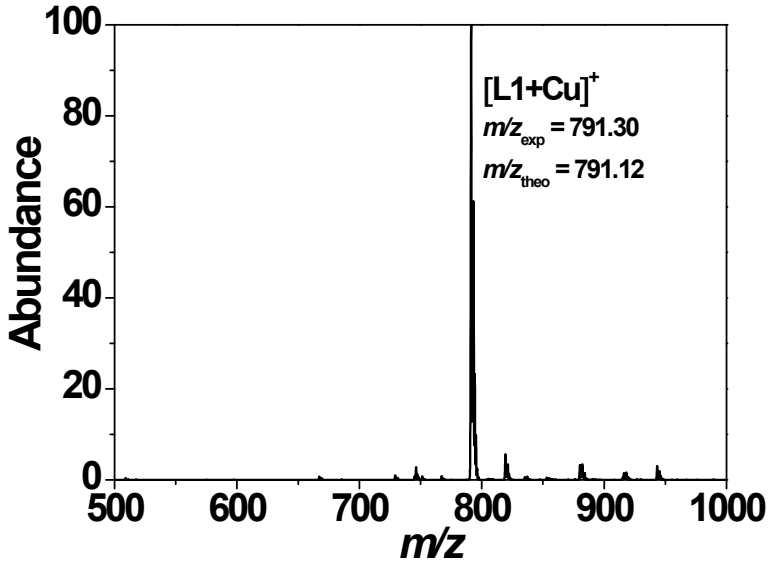

Figure S23. ESI mass spectra of the cupric complexes formed with ligand **L1**. Solvent: CH_3CN/CH_3OH (1/1 *v/v*); positive mode. (a) $[Cu^{2+}]_0 = [\mathbf{L1}]_0 = 5 \times 10^{-5}$ M; $V_c = 150$ V. The ESI-MS spectra were limited to the areas of interest. No peaks of interest were detected in the excluded *m/z* regions. For the $[\mathbf{L1}+Cu]^+$, it is suggested that the copper cation is reduced.

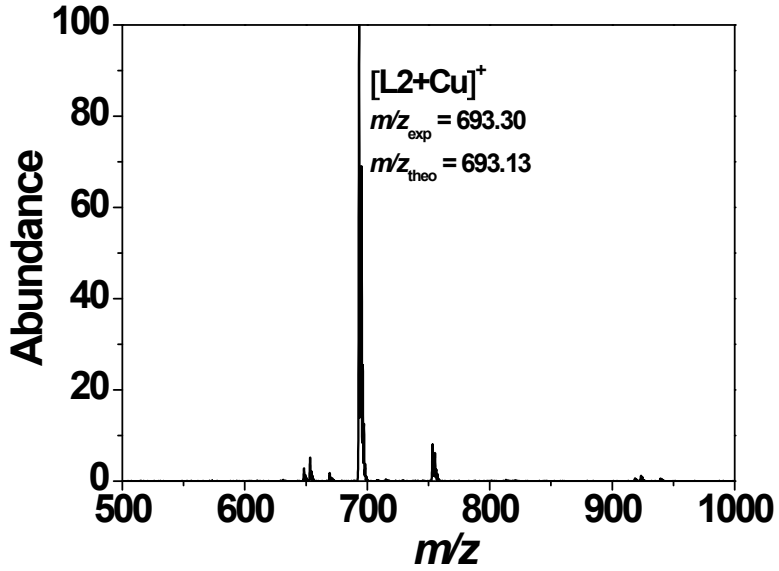

Figure S24. ESI mass spectra of the cupric complexes formed with ligand **L2**. Solvent: CH_3CN/CH_3OH (1/1 *v/v*); positive mode. (a) $[Cu^{2+}]_0 = [\mathbf{L2}]_0 = 5 \times 10^{-5}$ M; $V_c = 150$ V. The ESI-MS spectra were limited to the areas of interest. No peaks of interest were detected in the excluded *m/z* regions. For the $[\mathbf{L2}+Cu]^+$, it is suggested that the copper cation is reduced.

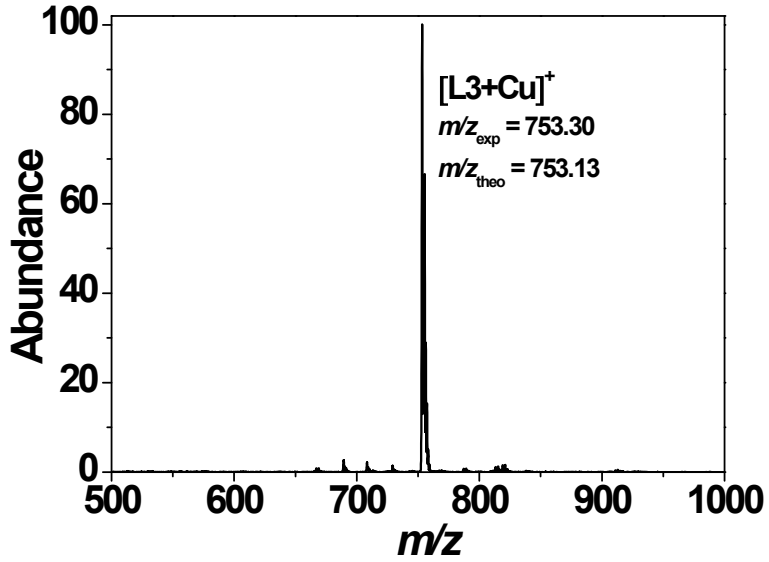

Figure S25. ESI mass spectra of the cupric complexes formed with ligand **L3**. Solvent: CH_3CN/CH_3OH (1/1 *v/v*); positive mode. (a) $[Cu^{2+}]_0 = [\mathbf{L3}]_0 = 5 \times 10^{-5}$ M; $V_c = 150$ V. The ESI-MS spectra were limited to the areas of interest. No peaks of interest were detected in the excluded *m/z* regions. For the $[\mathbf{L3}+Cu]^+$, it is suggested that the copper cation is reduced.

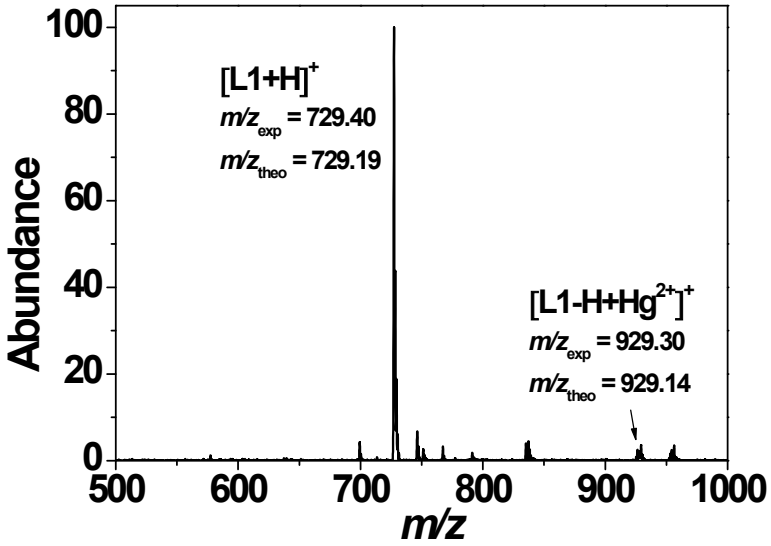

Figure S26. ESI mass spectra of the mercuric complexes formed with ligand **L1**. Solvent: CH_3CN/CH_3OH (1/1 *v/v*); positive mode. (a) $[Hg^{2+}]_0 = 1.5 \times 10^{-4}$ M; $[\mathbf{L1}]_0 = 5 \times 10^{-5}$ M; $V_c = 150$ V. The ESI-MS spectra were limited to the areas of interest. No peaks of interest were detected in the excluded *m/z* regions.

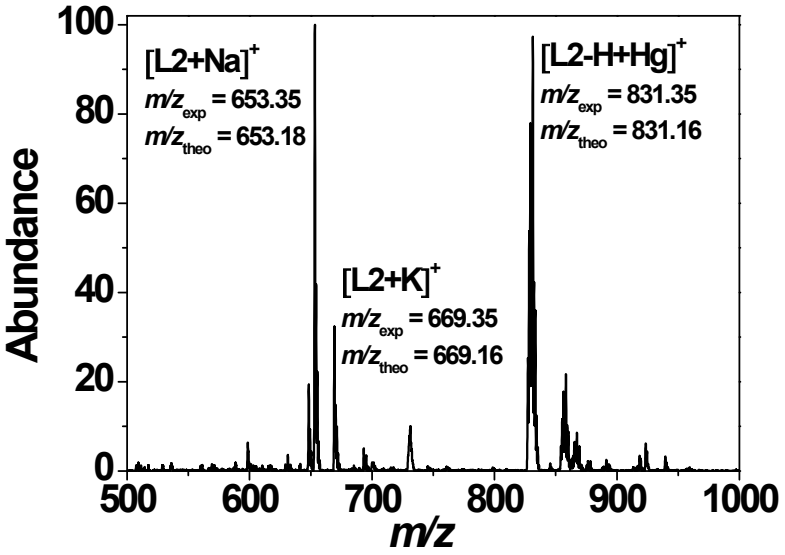

Figure S27. ESI mass spectra of the mercuric complexes formed with ligand **L2**. Solvent: CH_3CN/CH_3OH (1/1 *v/v*); positive mode. (a) $[Hg^{2+}]_0 = [\mathbf{L2}]_0 = 5 \times 10^{-5}$ M; $V_c = 150$ V. The ESI-MS spectra were limited to the areas of interest. No peaks of interest were detected in the excluded *m/z* regions.

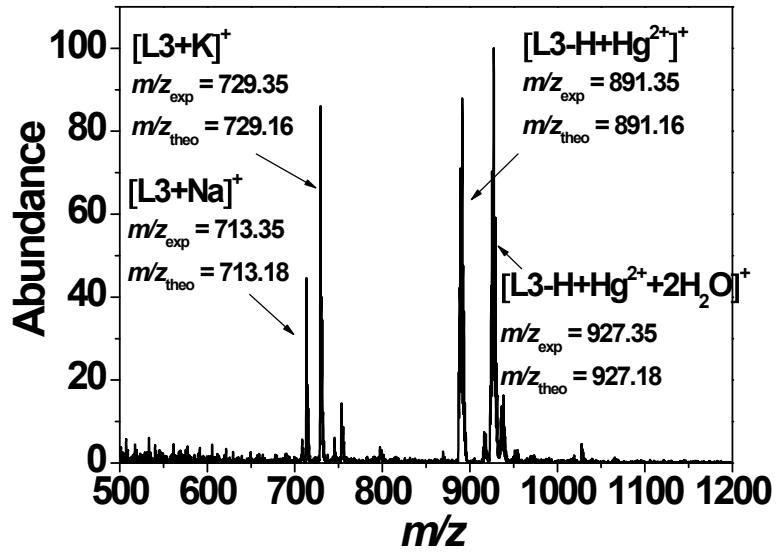

Figure S28. ESI mass spectra of the mercuric complexes formed with ligand **L3**. Solvent: CH_3CN/CH_3OH (1/1 *v/v*); positive mode. (a) $[Hg^{2+}]_0 = [\mathbf{L3}]_0 = 5 \times 10^{-5}$ M; $V_c = 150$ V. The ESI-MS spectra were limited to the areas of interest. No peaks of interest were detected in the excluded *m/z* regions.

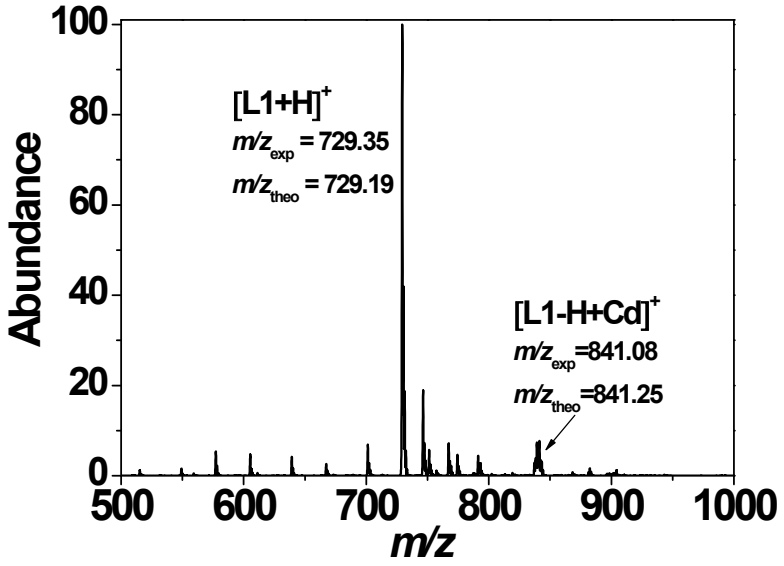

Figure S29. ESI mass spectra of the cadmium(II) complexes formed with ligand **L1**. Solvent: CH_3CN/CH_3OH (1/1 *v/v*); positive mode. (a) $[Cd^{2+}]_0 = [\mathbf{L1}]_0 = 5 \times 10^{-5}$ M; $V_c = 200$ V. The ESI-MS spectra were limited to the areas of interest. No peaks of interest were detected in the excluded *m/z* regions.

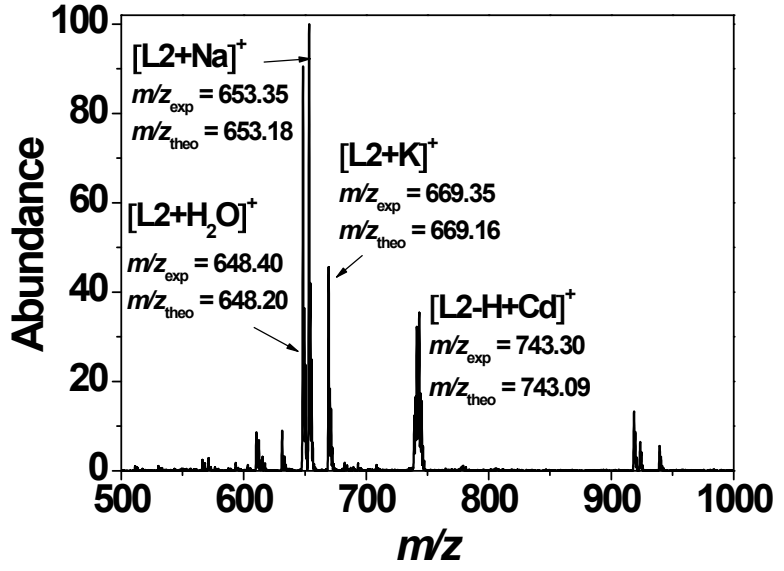

Figure S30. ESI mass spectra of the cadmium(II) complexes formed with ligand **L2**. Solvent: CH_3CN/CH_3OH (1/1 *v/v*); positive mode. (a) $[Cd^{2+}]_0 = 1.5 \times 10^{-4}$ M; $[\mathbf{L2}]_0 = 5 \times 10^{-5}$ M; $V_c = 150$ V. The ESI-MS spectra were limited to the areas of interest. No peaks of interest were detected in the excluded *m/z* regions. For the $[\mathbf{L2}+H_2O]^+$, it is suggested that one phenol is oxidized.

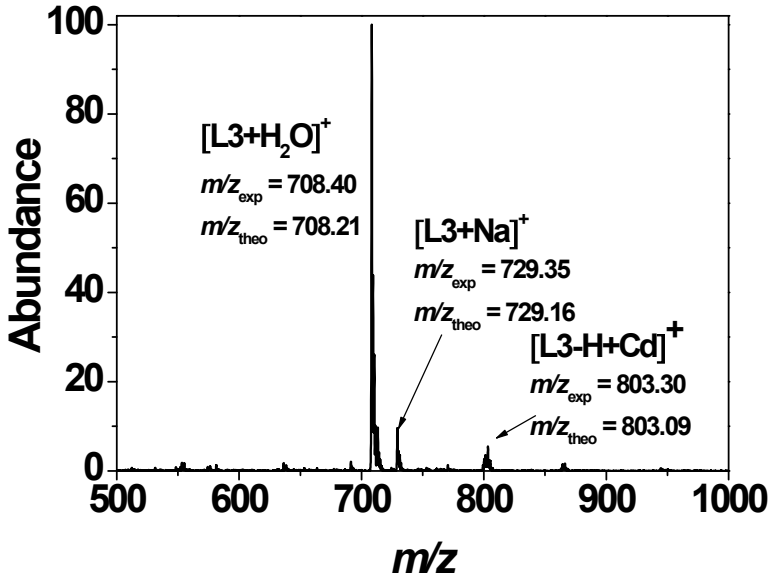

Figure S31. ESI mass spectra of the cadmium(II) complexes formed with ligand **L3**. Solvent: CH_3CN/CH_3OH (1/1 *v/v*); positive mode. (a) $[Cd^{2+}]_0 = 1.5 \times 10^{-4}$ M; $[\mathbf{L3}]_0 = 5 \times 10^{-5}$ M; $V_c = 150$ V. The ESI-MS spectra were limited to the areas of interest. No peaks of interest were detected in the excluded *m/z* regions. For the $[\mathbf{L3}+H_2O]^+$, it is suggested that one phenol is oxidized.

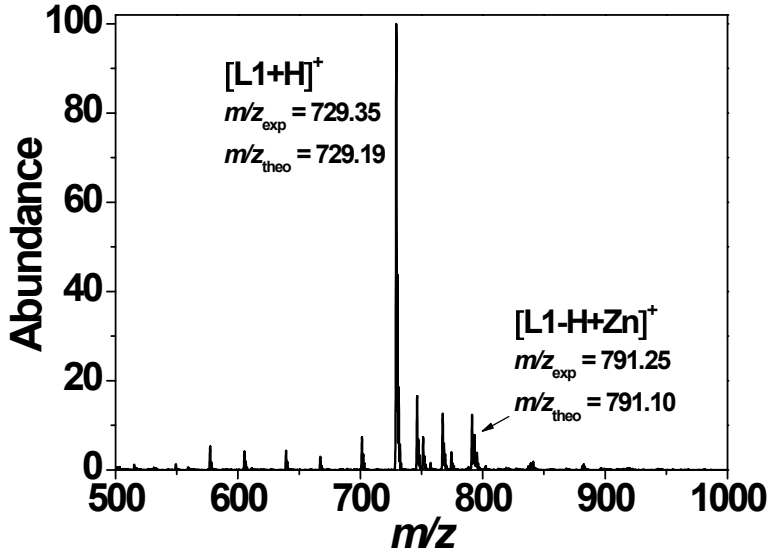

Figure S32. ESI mass spectra of the zinc(II) complexes formed with ligand **L1**. Solvent: CH_3CN/CH_3OH (1/1 *v/v*); positive mode. (a) $[Zn^{2+}]_0 = [\mathbf{L1}]_0 = 5 \times 10^{-5}$ M; $V_c = 200$ V. The ESI-MS spectra were limited to the areas of interest. No peaks of interest were detected in the excluded *m/z* regions.

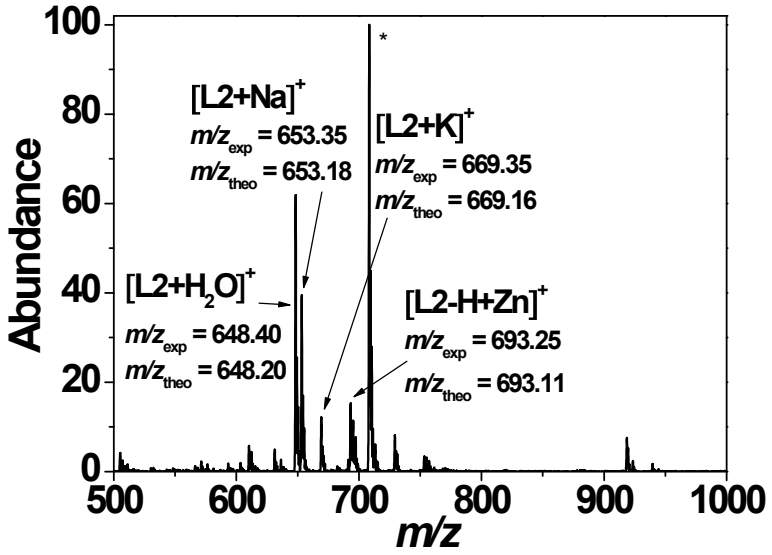

Figure S33. ESI mass spectra of the zinc(II) complexes formed with ligand **L2**. Solvent: CH_3CN/CH_3OH (1/1 *v/v*); positive mode. (a) $[Zn^{2+}]_0 = 3\times 10^{-4}$ M; $[\mathbf{L2}]_0 = 5 \times 10^{-5}$ M; $V_c = 150$ V. The ESI-MS spectra were limited to the areas of interest. No peaks of interest were detected in the excluded *m/z* regions. For the $[\mathbf{L2}+H_2O]^+$, it is suggested that one phenol is oxidized. * An intense peak at *m/z* 708.40 could not be characterized.

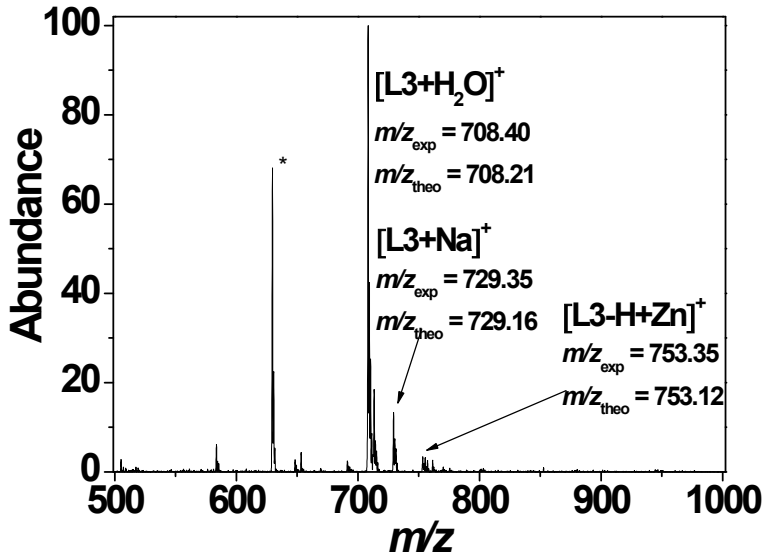

Figure S34. ESI mass spectra of the zinc(II) complexes formed with ligand **L3**. Solvent: CH_3CN/CH_3OH (1/1 *v/v*); positive mode. (a) $[Zn^{2+}]_0 = 1.5 \times 10^{-4}$ M; $[\mathbf{L3}]_0 = 5 \times 10^{-5}$ M; $V_c = 150$ V. The ESI-MS spectra were limited to the areas of interest. No peaks of interest were detected in the excluded *m/z* regions. For the $[\mathbf{L3}+H_2O]^+$, it is suggested that one phenol is oxidized. * An intense peak at *m/z* 629.70 could not be characterized.

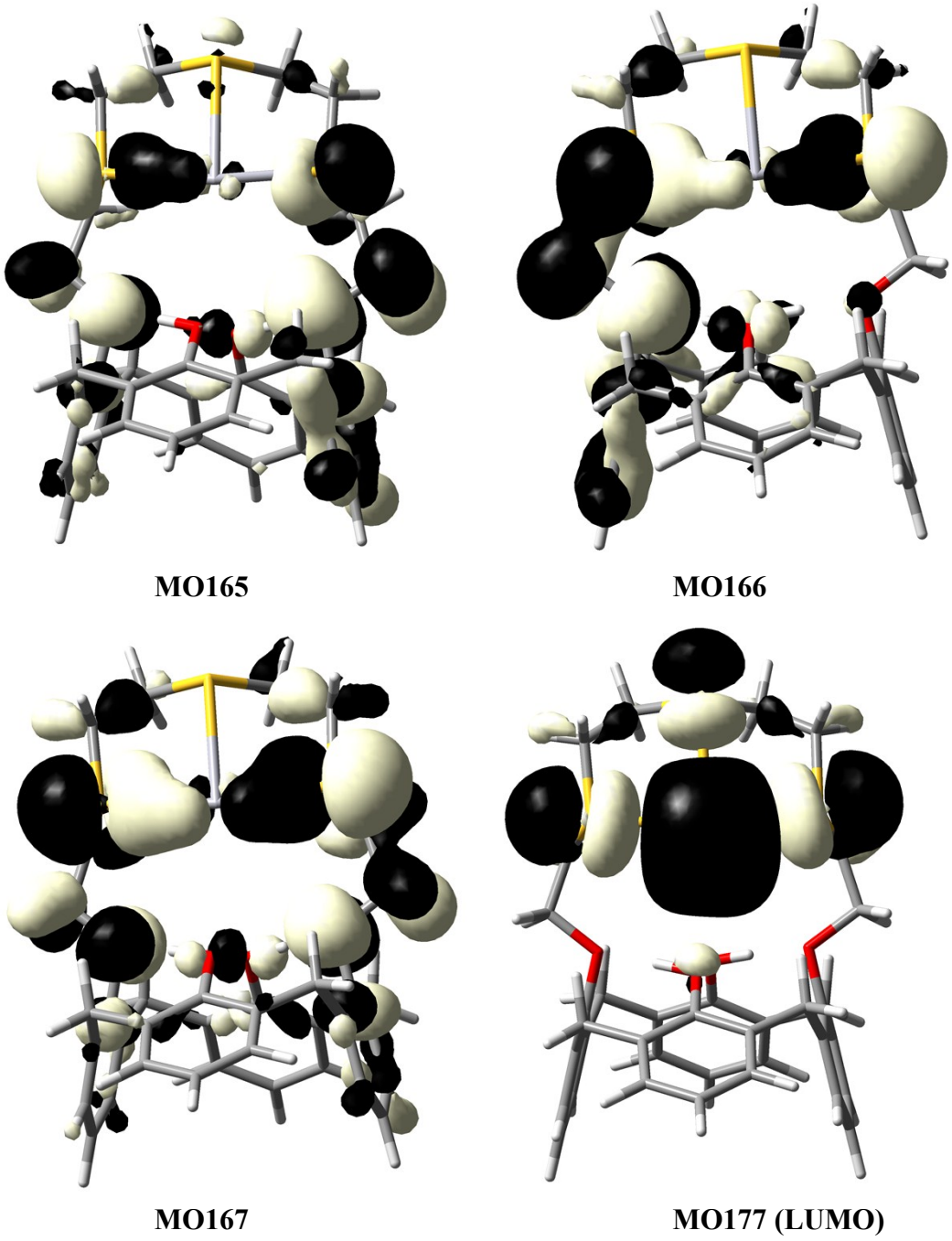

Figure S35. Calculated isosurfaces (0.02 a. u.) for MOs 165, 166, 167 and 177 (LUMO) of [Hg**L2**]$^{2+}$ (TPSSh/TZVP, acetonitrile solution).

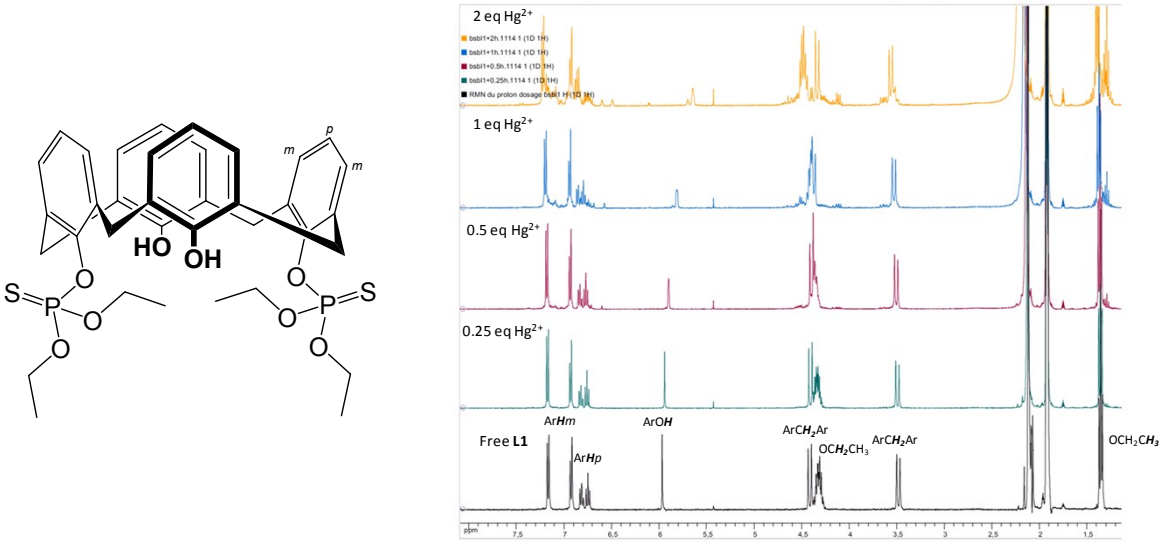

Figure S36. ^{1}H NMR titration of ligand **L^{1}** by Hg^{2+}. Solvent: CD_3CN; $[\mathbf{L1}]_0 = 2 \times 10^{-3}$ M; T = 298°C.

Table S1. Optimized (TPSSh/TZVP) bond distances of the metal coordination environments in the mercuric complexes with ligands **L1**, **L2** and **L3**.

	$[HgL1]^{2+}$	$[HgL2]^{2+}$	$[HgL3]^{2+}$
Hg1-S(1)	2.433	2.592	2.591
Hg1-S(2)	2.432	2.630	2.607
Hg1-S(3)	-	2.807	2.787
Hg1-S(4)	-	-	2.730

Table S2. Optimized (TPSSh/SVP) bond distances of the metal coordination environments in the cupric complexes with ligands **L1**, **L2** and **L3**.

	$[CuL1]^{2+}$	$[CuL2]^{2+}$	$[CuL3]^{2+}$
Cu1-O(1)	2.157	-	-
Cu1-O(2)	2.230	-	-
Cu1-O(3)	2.621	-	-
Cu1-O(4)	2.153	2.134	-
Cu1-S(1)	2.419	2.394	2.410
Cu1-S(2)	2.373	2.427	2.403
Cu1-S(3)	-	2.405	2.367
Cu1-S(4)	-	-	2.356